# Spin-orbit torques in $L1_0$-FePt/Pt thin films driven by electrical and thermal currents

Guillaume Géranton,* Frank Freimuth, Stefan Blügel, and Yuriy Mokrousov
*Peter Grünberg Institut and Institute for Advanced Simulation, Forschungszentrum Jülich and JARA, 52425 Jülich, Germany*
(Received 5 September 2014; revised manuscript received 17 December 2014; published 14 January 2015)

Using the linear response formalism, we compute from first principles the spin-orbit torque (SOT) in a system of two layers of $L1_0$-FePt(001) deposited on an fcc Pt(001) substrate of varying thickness. We find that at room temperature the values of the SOTs that are even and odd with respect to magnetization generally lie in the range of values measured and computed for Co/Pt bilayers. We also observe that the even SOT is much more robust with respect to changing the number of layers in the substrate, and as a function of energy it follows the general trend of the even SOT exerted by the spin Hall current in fcc Pt. The odd torque, on the other hand, is strongly affected by modification of the electronic structure for a specific energy window in the limit of very thin films. Moreover, taking the system at hand as an example, we compute the values of the thermal spin-orbit torque (TSOT). We predict that the gradients of temperature which can be experimentally created in this type of system will cause a detectable torque on the magnetization. We also underline the correlation between the even TSOT and the spin Nernst effect, thus motivating a more intensive experimental effort aimed at an observation of both phenomena.

DOI: 10.1103/PhysRevB.91.014417 PACS number(s): 72.25.Ba, 72.25.Mk, 71.70.Ej, 75.70.Tj

## I. INTRODUCTION

The possibility of manipulating the magnetization of a ferromagnet by spin-polarized electric currents was first pointed out by Berger [1] and Slonczewski [2]. After its experimental observation in 1999 [3] there has been growing interest in making use of this phenomenon in spintronics devices, e.g., for switching the magnetization in spin valves. Spin-transfer torque random-access memory (STT-MRAM) has the advantages of better scalability and lower power consumption over conventional magnetoresistive random-access memory (MRAM), where the information is written by an external magnetic field. However, the current density required to switch the magnetization is preventing STT-MRAM size from scaling down, and overcoming this problem is a central aim of current research efforts in the field of spintronics. Thus, it has become necessary to develop an understanding of the interplay between the magnetization and the currents driven by electric fields, as well as temperature gradients.

While spin-transfer torques rely on the exchange of spin angular momentum between two magnets with different direction of the magnetization, the so-called spin-orbit torques (SOTs) have been discovered only recently [4–6], and they are attributed to the spin-orbit-mediated exchange of angular momentum between the crystal lattice and the magnetization. This type of torque exists also in systems with collinear magnetization when inversion symmetry is broken [7,8], and it has been shown that SOTs can lead to the reversal of the ferromagnetic magnetization without the help of an additional polarizing layer [9–11]. Moreover, SOTs were shown to lead to a very fast domain wall motion in thin films at low current density [5,12,13]. This suggests that SOTs could play a crucial role in the next generation of spintronics devices.

On the theoretical side, two mechanisms have been proposed that give rise to SOTs in heavy metal/ferromagnetic bilayers. The first one is due to the torque exerted on the magnetization by the spin current from the spin Hall effect (SHE) of the heavy metal. The second one is due to the nonequilibrium spin density that is generated at the interface when the distribution function of the system is driven out of equilibrium by an electric field. While the sign and the amplitude of the SOTs due to the SHE are commonly estimated from the bulk spin Hall conductivity of the heavy metal, quantitative predictions of the second contribution are generally based on the Rashba model [7]. Such simplified approaches are unable to explain the sensitivity of the SOT to the substrate thickness or microscopic details of the interface [14]. Recently, a first-principles method to compute SOTs based on the general linear response formalism was developed [15], which allows us to fully take into account the fine details of the electronic structure that are crucial for determining the SOT in transition-metal multilayers with high accuracy. The first application of this method to Co/Pt bilayers has shown very good agreement with experiment. More recently, the theory of the SOT arising in response to thermal gradients has been also developed [16]. This allows us to access this spincaloric effect from *ab initio*.

Perpendicular magnetic anisotropy is desirable for various applications in, e.g., data storage [17]. Many ferromagnetic multilayers of 3*d* transition metals with heavy transition metals are known to exhibit very large magnetocrystalline anisotropy energy (MAE) that favors out-of-plane magnetization [18], and among materials of this type Co/Pt bilayers are most studied experimentally with respect to SOT [6,9,11]. However, the large lattice mismatch between Co and Pt results in a rather poor quality of the interface in these systems. For disentangling various contributions to the SOT and for comparison between theoretical results with experiments in this kind of system, the high quality of the interface is of utmost importance. In this paper, we therefore study from first principles the SOT in $L1_0$-FePt/Pt bilayers, which have a large out-of-plane MAE [19], and which can be grown epitaxially, thus exhibiting high interfacial crystallinity [20,21].

*g.geranton@fz-juelich.de

 

The goal of this paper is twofold. First, we compute and analyze different contributions to the SOT in $L1_0$-FePt/Pt thin films as a function of Pt thickness [15]. We analyze the energy dependence of the SOT and relate it to the energy dependence of the bulk spin Hall effect in Pt. Second, taking FePt/Pt bilayers as an example, we present *ab initio* calculations of thermal SOT (TSOT), i.e., the SOT which is driven by a temperature gradient rather than an electric field. We briefly outline the ways how the TSOT can be enhanced. Finally, we show that the energy dependence and magnitude of the even TSOT can be estimated from the spin Nernst effect in bulk Pt.

## II. FORMALISM

We investigate the SOT in our system using expressions obtained from the Kubo linear response formalism, and evaluated based on the electronic structure computed within density functional theory. Within linear response the torque $\mathbf{T}$ exerted on the ferromagnetic magnetization when an electric field $\mathbf{E}$ is applied is given by $\mathbf{T} = \mathbf{t}\mathbf{E}$. The torkance tensor $\mathbf{t}$ has three contributions [15],

$$
\begin{aligned}
t_{ij}^{\mathrm{I(a)}} &= -\frac{e}{h}\int_{-\infty}^{\infty} d\mathcal{E}\frac{df(\mathcal{E})}{d\mathcal{E}}\mathrm{Tr}\langle \mathcal{T}_i G^{\mathrm{R}}(\mathcal{E}) v_j G^{\mathrm{A}}(\mathcal{E})\rangle,\\
t_{ij}^{\mathrm{I(b)}} &= \frac{e}{h}\int_{-\infty}^{\infty} d\mathcal{E}\frac{df(\mathcal{E})}{d\mathcal{E}}\mathrm{Re}\,\mathrm{Tr}\langle \mathcal{T}_i G^{\mathrm{R}}(\mathcal{E}) v_j G^{\mathrm{R}}(\mathcal{E})\rangle,\\
t_{ij}^{\mathrm{II}} &= \frac{e}{h}\int_{-\infty}^{\infty} d\mathcal{E}\, f(\mathcal{E})\mathrm{Re}\,\mathrm{Tr}\Big\langle \mathcal{T}_i G^{\mathrm{R}}(\mathcal{E}) v_j \frac{dG^{\mathrm{R}}(\mathcal{E})}{d\mathcal{E}}\\
&\quad -\mathcal{T}_i \frac{dG^{\mathrm{R}}(\mathcal{E})}{d\mathcal{E}} v_j G^{\mathrm{R}}(\mathcal{E})\Big\rangle,
\end{aligned}
\tag{1}
$$

with $G^{\mathrm{R}}(\mathcal{E})$ and $G^{\mathrm{A}}(\mathcal{E})$ as the retarded and advanced Green's functions, $v_j$ as the $j$th Cartesian component of the velocity operator, $\mathcal{T}_i$ as the $i$th Cartesian component of the torque operator, $f(\mathcal{E})$ as the Fermi distribution function, and $e > 0$ as the elementary positive charge. The torque operator is given by $\boldsymbol{\mathcal{T}} = -\mu_B \boldsymbol{\sigma} \times \mathbf{B}^{\mathrm{xc}}$, where $\boldsymbol{\sigma}$ and $\mathbf{B}^{\mathrm{xc}}$ are the vectors of Pauli spin matrices and the exchange field, respectively. We model the influence of disorder in the system by a constant effective band broadening, which was used successfully in the past for the study of the conductivity [22,23] and the magneto-optical Kerr effect [24]. Within this model the retarded and advanced Green's functions are given by $G^{\mathrm{R}}(\mathcal{E}) = \hbar[\mathcal{E} - H + i\Gamma]^{-1}$ and $G^{\mathrm{A}}(\mathcal{E}) = \hbar[\mathcal{E} - H - i\Gamma]^{-1}$, with parameter $\Gamma$ characterizing the disorder strength.

We decompose the torkance tensor $\mathbf{t}$ into even and odd components with respect to the direction of magnetization $\hat{\mathbf{M}}$: $t_{ij} = t_{ij}^{\mathrm{even}} + t_{ij}^{\mathrm{odd}}$. It is very insightful to consider the limit $\Gamma \to 0$. In this so-called clean limit the even and odd components of the torkance tensor acquire qualitatively different forms:

$$
t_{ij}^{\mathrm{even}} = \frac{2e}{\mathcal{N}}\hat{\mathbf{e}}_i \cdot \sum_{\mathbf{k},n} f(\epsilon_{\mathbf{k}n})\left[\hat{\mathbf{M}} \times \mathrm{Im}\left\langle \frac{\partial u_{\mathbf{k}n}}{\partial \hat{\mathbf{M}}} \,\middle|\, \frac{\partial u_{\mathbf{k}n}}{\partial k_j}\right\rangle\right] \tag{2}
$$

and

$$
t_{ij}^{\mathrm{odd}} = -\frac{e\hbar}{2\Gamma\mathcal{N}}\sum_{\mathbf{k}n}\langle\psi_{\mathbf{k}n}|\mathcal{T}_i|\psi_{\mathbf{k}n}\rangle\langle\psi_{\mathbf{k}n}|v_j|\psi_{\mathbf{k}n}\rangle\frac{\partial f(\epsilon_{\mathbf{k}n})}{\partial \mathcal{E}}, \tag{3}
$$

where $\mathbf{k}$ is the Bloch vector in the Brillouin zone with an overall number $\mathcal{N}$, $n$ runs over all bands, $\epsilon_{\mathbf{k}n}$ are the eigenenergies of the system, $\psi_{\mathbf{k}n}$ and $u_{\mathbf{k}n}$ are the Bloch states and their lattice-periodic parts, respectively, and $\hat{\mathbf{e}}_i$ is the unit vector along the $i$th Cartesian direction. In contrast to the conductivity tensor [25], it is in general not possible to identify the even and odd torkances with the symmetric or antisymmetric parts of the torkance tensor, which implies that all components of the torkance tensor can have both even and odd contributions. As discussed in other works by the authors [15], the even torkance has the form of a Berry curvature and it is independent of $\Gamma$ in the limit of $\Gamma \to 0$. It constitutes the intrinsic contribution to the torkance, and it is analogous to the intrinsic anomalous or spin Hall effects. The odd part of the torkance, on the other hand, diverges as $1/\Gamma$ in the limit of small $\Gamma$, i.e., it is proportional to the quasiparticle lifetime in analogy to the Rashba torque [7] or the diagonal electrical conductivity, and it is thus dependent on the scattering mechanisms present in the system.

Similarly to the spin Hall or anomalous Hall conductivities, the torkance tensor describes the SOT arising from an applied electric field, i.e., it corresponds to the situation where the torque is driven by a mechanical force. A torque can also be induced by a temperature gradient $\nabla T$, i.e., it can also originate from statistical forces. Within linear response this thermal torque reads

$$
\mathbf{T} = -\boldsymbol{\beta}\nabla T, \tag{4}
$$

where $\boldsymbol{\beta}$ is the *thermal torkance*. In analogy to the torkance driven by electrical currents, we decompose the thermal torkance into even and odd components with respect to the magnetization direction. The intrinsic even part of the thermal torkance is analogous to the intrinsic anomalous Nernst [26,27] and spin Nernst conductivities [28–31]. Similar to the latter effects, it can be shown that the thermal torkance $\beta$ can be computed directly from its mechanical counterpart by employing the Mott relation [16]

$$
\beta_{ij}(T) = -\frac{1}{e}\int d\mathcal{E}\frac{\partial f(\mathcal{E},\mu,T)}{\partial \mu} t_{ij}(\mathcal{E})\frac{\mathcal{E}-\mu}{T}, \tag{5}
$$

where $t_{ij}(\mathcal{E})$ is the torkance tensor with the Fermi energy set to $\mathcal{E}$ and $\mu$ is the chemical potential. In this paper, we compute both electrical and thermal SOTs based on the *ab initio* electronic structure of FePt/Pt bilayers according to Eqs. (1) and (5).

At low temperature, the derivative of the Fermi distribution function is significant only very close to the chemical potential $\mu$. Performing a Taylor expansion of the integrand $t_{ij}(\mathcal{E})\frac{\mathcal{E}-\mu}{T}$ about $\mathcal{E} = \mu$ up to the second order, one obtains the zero temperature limit expression for the thermal torkance,

$$
\beta_{ij}(T) = -\frac{\pi^2 k_B^2 T}{3e}\frac{\partial t_{ij}}{\partial \mathcal{E}}\bigg|_{\mathcal{E}=\mu}, \tag{6}
$$

which shows that the thermal torkance for a given chemical potential $\mu$ is proportional to the derivative of the torkance tensor at $\mathcal{E} = \mu$.

## III. COMPUTATIONAL DETAILS AND BASIC PROPERTIES

In our study we considered two layers of $L1_0$-FePt oriented along the [001] direction and terminated with Fe atoms (Fe/Pt/Fe/Pt/Fe) deposited on the upper side of a Pt(001) film with a thickness of six, 12, and 18 layers. The electronic structure of these $L1_0$-FePt/Pt(001) thin films was computed within the density functional theory (DFT) using the Perdew, Burke, and Ernzerhof (PBE) functional and the full-potential linearized augmented-plane-wave method as implemented in the two-dimensional version of the code FLEUR [32]. DFT calculations were performed with 576 $k$-points in the two-dimensional Brillouin zone. The plane-wave cutoff was set to $3.7a_0^{-1}$ and the muffin-tin radii to $2.4a_0$, where $a_0$ is the Bohr radius. The in-plane lattice constant of the films $a$ was set to 2.7765 Å (see Fig. 1). This value is equal to $1/\sqrt{2}$ times the experimental lattice constant of fcc Pt (3.9265 Å) and therefore corresponds to the situation where $L1_0$-FePt is grown epitaxially on the Pt substrate. The relaxation of the out-of-plane distances between atomic layers $d_z$ was performed until the forces were smaller than $10^{-5}$ hartree/$a_0$. See Table I for a list of the relaxed interlayer distances.

For out-of-plane magnetization the computed spin moments of Fe atoms range between $3.02\mu_B$ and $3.08\mu_B$ depending on the thickness and position of the Fe atom with respect to the interface with the Pt substrate. The largest spin moment of the Pt atoms is about $0.4\mu_B$ in the FePt overlayer, while the largest spin moment among the substrate atoms is $0.3\mu_B$ for the Pt atom closest to the interface. Spin moments then rapidly decay when going further in the substrate (see also Table I). For the thinnest film we have also computed the value of the magnetocrystalline anisotropy energy and found it to be 1.2 meV per Fe atom, favoring out-of-plane magnetization, while the anisotropy within the plane was one order of magnitude smaller.

To compute the SOTs we employed the Wannier interpolation technique. We constructed 18 maximally localized Wannier functions (MLWFs) per atom from Bloch functions on an $8 \times 8$ $k$-point mesh using the WANNIER90 program [33,34]. The number of bands used to disentangle the subspace of the MLWFs was chosen such that for each film the ratio of the number of bands to the number of MLWFs was approximately equal to 1.4. This allows a very precise interpolation of the electronic structure up to 5 eV above the Fermi energy. The torkances were computed on a $2048 \times 2048$ $k$-point mesh, except for the case of $\Gamma$ well below 25 meV, where a $4096 \times 4096$ $k$-point mesh was used. For a system with $C_4$ symmetry and out-of-plane magnetization the torkance tensor has only two nonvanishing independent components, $t_{yx}^{\text{even}} = -t_{xy}^{\text{even}}$ and $t_{xx}^{\text{odd}} = t_{yy}^{\text{odd}}$, which are respectively even and odd functions of the magnetization direction. See Fig. 1 for the definition of the axes.

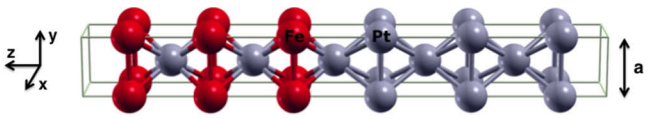


FIG. 1. (Color online) Illustration of the unit cell of a system of two layers of $L1_0$-FePt oriented along the [001] direction and terminated with Fe atoms (Fe/Pt/Fe/Pt/Fe) deposited on a Pt(001) film of six layers. Fe and Pt atoms are shown in red and gray, respectively. The in-plane lattice constant is $a = 2.7765$ Å.

TABLE I. Computational details for the thinnest film: interlayer distances $d_z$ from one atomic layer to the next one (in units of Å); variation $\Delta = (d_z - d_{\text{ref}})/d_{\text{ref}}$ of the interlayer distances with $d_{\text{ref}} = d_z(\text{Fe2})$ for the first five atomic layers and $d_{\text{ref}} = d_z(\text{Pt5})$ for the other ones; spin magnetic moments $\mu_{\text{at}}$ per atom (in units of $\mu_B$).

| Atomic layer | $d_z$ | $\Delta$ (%) | $\mu_{\text{at}}$ |
|---|---|---|---|
| Fe1 | 1.790 | −3.9 | 3.080 |
| Pt1 | 1.869 | 0.4 | 0.403 |
| Fe2 | 1.862 | 0.0 | 3.021 |
| Pt2 | 1.874 | 0.6 | 0.383 |
| Fe3 | 1.816 | −2.5 | 3.040 |
| Pt3 | 2.100 | 3.6 | 0.297 |
| Pt4 | 2.039 | 0.6 | 0.047 |
| Pt5 | 2.027 | 0.0 | 0.022 |
| Pt6 | 2.019 | −0.4 | 0.009 |
| Pt7 | 1.982 | −2.2 | 0.008 |
| Pt8 | | | 0.007 |

## IV. RESULTS

### A. Spin-orbit torques driven by electrical currents

We first compute the even and odd torkance as a function of the disorder strength $\Gamma$ and thickness of the Pt substrate using the expressions from Sec. II. The results of these calculations are presented in Fig. 2 and summarized in Table II for the band broadening of $\Gamma = 25$ meV $\approx k_B T_0$, which mimics the effect of room temperature $T_0$. At small $\Gamma$ the even torkance $t_{yx}^{\text{even}}$ is given by its clean limit Berry curvature value which lies in the range of 0.65–0.85$ea_0$ depending on the substrate thickness, and the deviation of $t_{yx}^{\text{even}}(\Gamma)$ from these values becomes significant only for band broadening larger than 100 meV. At larger $\Gamma$ the values of $t_{yx}^{\text{even}}$ for different numbers of Pt layers are almost identical to each other, meaning that the fine difference in the electronic structure of the films is washed out by the broadening of this magnitude. At $\Gamma = 25$ meV the

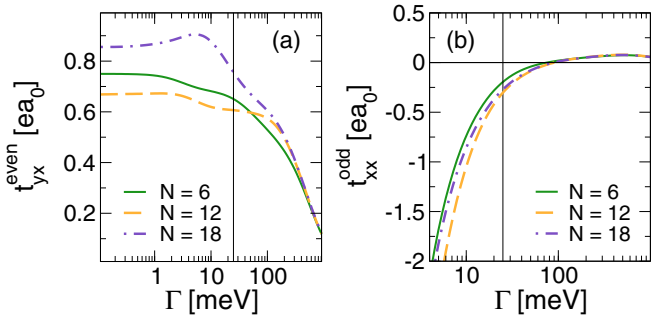


FIG. 2. (Color online) (a) Even torkance $t_{yx}^{\text{even}}$ and (b) odd torkance $t_{xx}^{\text{odd}}$ in $L1_0$-FePt$^2$/Pt$^N$ for $N = 6$ (green solid), 12 (orange dashed), and 18 (blue dotted-dashed), as a function of the disorder strength $\Gamma$. Solid vertical lines correspond to the value of $\Gamma = 25$ meV.

TABLE II. Even and odd torkances $t$ computed at $\Gamma = 25$ meV (in units of $ea_0$); even ($T_y^{\text{even}}/\mu_s$) and odd ($T_x^{\text{odd}}/\mu_s$) effective magnetic fields (in units of mT) for an applied electric field $E_x = 360$ V/cm; even and odd thermal torkances $\beta$ (in units of $\mu$eV $a_0$ K$^{-1}$); $|\nabla T|^0$ (in units of K/nm) is the temperature gradient required to reproduce the total effective magnetic field $\sqrt{(T_x^{\text{odd}})^2 + (T_y^{\text{even}})^2}/\mu_s$.

| | $FePt^2/Pt^6$ | $FePt^2/Pt^{12}$ | $FePt^2/Pt^{18}$ |
|---|---|---|---|
| $t_{yx}^{\text{even}}$ | +0.65 | +0.61 | +0.75 |
| $t_{xx}^{\text{odd}}$ | −0.19 | −0.30 | −0.27 |
| $T_y^{\text{even}}/\mu_s$ | +2.1 | +2.0 | +2.4 |
| $T_x^{\text{odd}}/\mu_s$ | −0.6 | −1.0 | −0.9 |
| $\beta_{yx}^{\text{even}}$ | −10.6 | −15.3 | −14.5 |
| $\beta_{xx}^{\text{odd}}$ | −4.8 | +0.7 | −2.5 |
| $\lvert\nabla T\rvert^0$ | +2.1 | +1.6 | +1.7 |

even torkance is still relatively close to the Berry curvature values (see also Table II), and the variation in $t_{yx}^{\text{even}}$ caused by Pt thickness is of the order of 15%. For this broadening the values of $t_{yx}^{\text{even}}$ for our system are rather close to those of $Co^3/Pt^{10}(111)$ bilayers, as computed in Ref. [15], which lie in the range of 0.53–0.62$ea_0$, depending on the capping.

As for the odd torkance, for broadenings below 10 meV, its magnitude is larger than that of the even torkance, while $t_{xx}^{\text{odd}}$ rapidly decays with $\Gamma$ and changes sign in the vicinity of $\Gamma \approx 80$ meV, where the difference in $t_{xx}^{\text{odd}}$ for films of different thicknesses is almost negligible. Overall, the characteristic $1/\Gamma$ behavior is clearly visible for small $\Gamma$. At room temperature the odd torkance is negative and it is roughly twice smaller in magnitude than the corresponding even torkance. The fact that $t_{xx}^{\text{odd}}$ is close to the point of changing the sign for $\Gamma = 25$ meV makes it also more sensitive to the Pt thickness, which otherwise does not have a pronounced effect on the odd torkance (see also Table II).

For comparing to experiments it is useful to represent the computed torkances in terms of the effective magnetic fields at a given current density, and in Table II we present the corresponding values of $T_y^{\text{even}}/\mu_s$ and $T_y^{\text{odd}}/\mu_s$ for an electric field $E_x$ of 360 V/cm, where $\mu_s$ stands for the total spin moment in the unit cell containing three Fe atoms with a value of about $10.1\mu_B$ for all thicknesses and out-of-plane magnetization. The value of the electric field ($E_x = 360$ V/cm) chosen to compute the effective magnetic fields corresponds to the current density $j \approx 10^7$ A/cm$^2$, if one assumes the resistivity to be $\rho = 36$ $\mu\Omega$ cm, which is the measured value for a similar Pt-based magnetic trilayer system, namely, Pt/Co/$AlO_x$ [35]. The values of the even effective magnetic fields of the order of 2.0 mT are generally consistent with those computed for Co/Pt bilayers [15], taking into account that the value of $\mu_s$ in the latter case is smaller by about 30% than that in the FePt/Pt bilayers that we study here.

It is instructive to compare the computed even SOT to the "hypothetical" torque $T_y$ that is exerted on the magnetization if the spin current density across the interface between the Pt substrate and the $L1_0$-FePt overlayer is given by the spin Hall conductivity of bulk fcc Pt. When an electric field $E_x$ is applied along the $x$ direction in Pt, a spin current with spin polarization in the $y$ direction flows in the $z$ dimension due to the SHE.

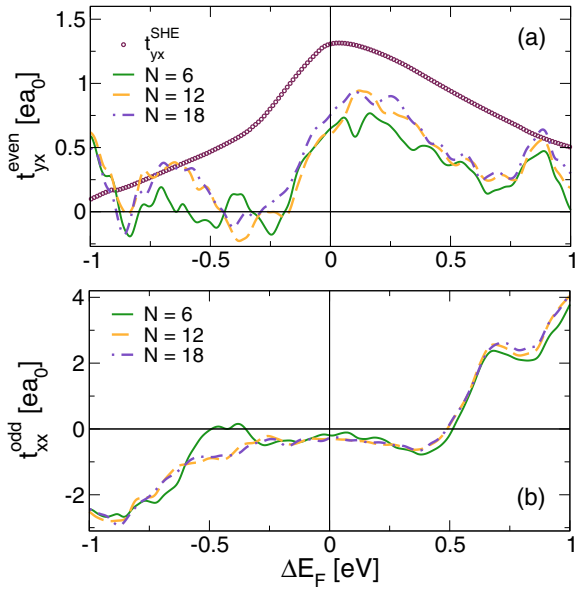


FIG. 3. (Color online) (a) Even torkance $t_{yx}^{\text{even}}$ and (b) odd torkance $t_{xx}^{\text{odd}}$ as a function of the Fermi energy (with respect to the true Fermi energy $E_F \approx -4.33$ eV for all three thicknesses) at $\Gamma = 25$ meV in $L1_0$-$FePt^2/Pt^N$ films for $N = 6$ (green solid), 12 (orange dashed), and 18 (blue dotted-dashed). The line of circles in the upper figure corresponds to the even torkance $t_{yx}^{\text{SHE}}$ estimated from the spin Hall conductivity of bulk fcc Pt, Eq. (7).

This spin current $j_z^y$ is given by $j_z^y = \sigma_{zx}^y E_x$, where $\sigma_{zx}^y$ is the SHE conductivity. Under the assumption that the whole of the bulk spin Hall current is transferred to the magnetization, i.e., that $T_y = Sj_z^y$, where $S = 7.71$ Å$^2$ is the in-plane area of the unit cell, this model yields a simple expression for the even torkance:

$$t_{yx}^{\text{SHE}} = S\sigma_{zx}^y. \tag{7}$$

In Fig. 3 we plot the even spin Hall torkance $t_{yx}^{\text{SHE}}$ in comparison to the even torkance $t_{yx}$ computed at $\Gamma = 25$ meV as a function of the Fermi energy in our system. To estimate $t_{yx}^{\text{SHE}}$ we used the intrinsic SHC in bulk fcc Pt (note that our calculations show that the influence of band smearing of the order of 25 meV on the bulk Pt SHC is negligible). At the true Fermi energy, the SHC of Pt is found to be 2184 $(\hbar/e)$S/cm. As is apparent from Fig. 3, in the interval of energies of $[-0.1, +0.5]$ eV with respect to the true Fermi energy, the even SOT can be approximated with the expression $t_{yx}^{\text{even}} = \xi t_{yx}^{\text{SHE}}$, where the so-called *SHE-to-SOT efficiency* $\xi$ [36] smoothly varies with energy in the range of $0.5 < \xi < 0.7$ and moderately depends on the Pt thickness. As a result, in this energy range the qualitative behavior of $t_{yx}^{\text{even}}$ quite closely resembles that of $t_{yx}^{\text{SHE}}$. In this energy region one could attribute the moderate energy and Pt thickness dependence of $\xi$ and its deviation from the "ideal" value of 1.0 to the finite size effects and details of the electronic structure which, e.g., influence the magnitude of the spin current generated in the Pt substrate, as well as its $z$ distribution inside the slab and transmission properties of the interface [36]. We note that the range of values of $\xi$ for energies between −0.1 and 0.5 eV is rather close to that computed in the presence of

disorder for Co/Pt bilayers. For the latter system it was shown that $t_{yx}^{\text{even}}$ arises mainly due to the spin current which originates from the SHE inside the Pt substrate [15]. On the other hand, away from this energy range, $t_{yx}^{\text{even}}$ in FePt/Pt can differ from $t_{yx}^{\text{SHE}}$ by an order of magnitude and even in sign (e.g., around $E_{\text{F}} = -0.35$ and $-0.8$ eV), which signifies that the application of simplified models of the kind of Eq. (7) has to be done with extreme caution.

Figure 3 shows that while the even torkance as a function of energy reaches its maximal values around the true Fermi energy of FePt/Pt, the values of the odd torkance are small around the true $E_{\text{F}}$, and they become very large away from it. As far as the thickness dependence of both $t_{yx}^{\text{even}}$ and $t_{xx}^{\text{odd}}$ is concerned, significant deviations between the torkances for $N = 6$ and larger thicknesses are visible only in the energy interval of about $-0.7$ to $-0.3$ eV. The difference in the torkances for $N = 12$ and 18 is, on the other hand, smaller. Among the two, the thickness dependence is more pronounced for the odd torkance, with the difference reaching as much as $1ea_0$ between $t_{xx}^{\text{odd}}$ for thin and thick films, while for $t_{yx}^{\text{even}}$ this difference is much smaller.

In Fig. 4 we present the band structures of the slabs with six and 18 layers of Pt in the substrate. The two band structures look very similar, with the only obvious difference lying in the increased number of bands for the thicker substrate. However, in the energy interval of interest, a relatively large hybridization of the states which have larger weight at the bottom layer of the Pt substrate with the states which exhibit larger weight at the interface between $L1_0$-FePt and Pt is clearly visible for the $L1_0$-FePt$^2$/Pt$^6$ film (see the black circles in Fig. 4), while this hybridization is almost absent for the $L1_0$-FePt$^2$/Pt$^{18}$ film. Thus, we speculate that the crosstalk between the free surface of the Pt substrate and the interface with FePt, which is almost decoupled for large Pt thicknesses, and quite pronounced for the six-layer film, could lead to significant differences in the SOTs of thin and thick FePt/Pt bilayers.

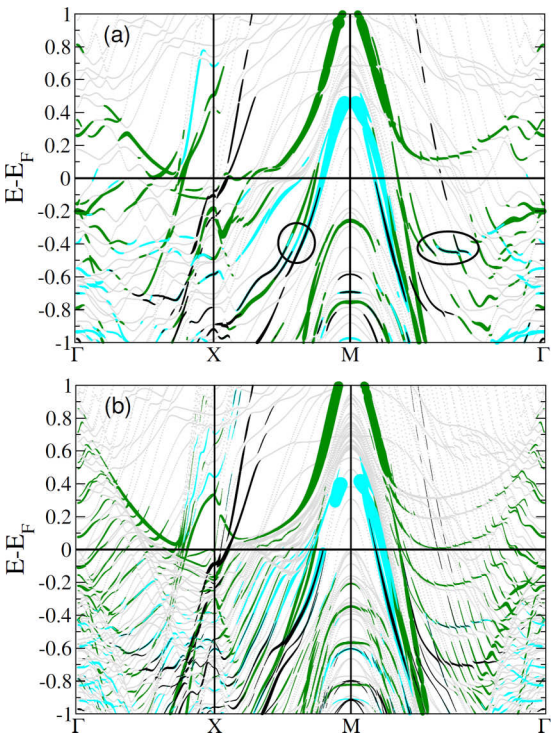


FIG. 4. (Color online) Band structures of (a) $L1_0$-FePt$^2$/Pt$^6$ and (b) $L1_0$-FePt$^2$/Pt$^{18}$ thin films along high symmetry lines. States with a large portion of the wave function on specific atoms are marked by green/dark gray (Pt atoms at the bottom of the slab), cyan/light gray (Pt substrate atoms closest to the FePt/Pt interface), and black (Fe atoms closest to the FePt/Pt interface). The criteria for a state to be marked is that (a) more than 9.6% for Pt atoms and 7.7% for Fe atoms of the charge of the state are localized inside a corresponding atom. For (b) these values constitute 4.5% for Pt atoms and 3.6% for Fe atoms, owing to the twice larger thickness. The radius of the dots is proportional to the weight of the wave function inside a corresponding atom. All states are marked by light gray dots in the background.

### B. Thermal spin-orbit torques

We compute the thermal spin-orbit torques (TSOTs) in our system according to Eq. (5) at a temperature $T = 300$ K using as the input the energy dependence of the even and odd torkances computed at $\Gamma = 25$ meV and presented in Fig. 3. The energy dependence of the even and odd thermal torkances $\beta_{yx}^{\text{even}}$ and $\beta_{xx}^{\text{odd}}$ of $L1_0$-FePt/Pt thin films at room temperature is shown in Fig. 5, and their values at the Fermi energy are summarized in Table II.

By direct inspection, it is easy to see that the trend of $\beta_{yx}^{\text{even}}$ and $\beta_{xx}^{\text{odd}}$ with energy can be directly related to the corresponding behavior of $t_{yx}^{\text{even}}$ and $t_{xx}^{\text{odd}}$. This follows from the observation that in the zero temperature limit the thermal torkance $\beta$ is proportional to the energy derivative of the torkance $t$ [see Eq. (6)]. Indeed, by comparing the curves in Figs. 5 and 3, we can see that in most of the cases the

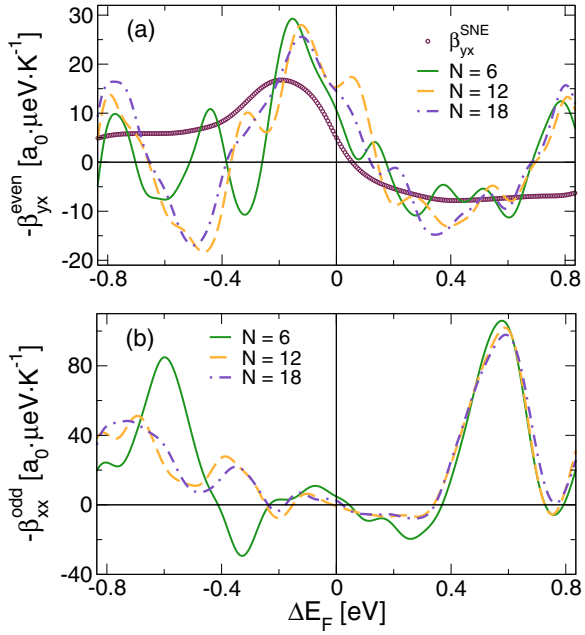


FIG. 5. (Color online) (a) Even thermal torkance $\beta_{yx}^{\text{even}}$ and (b) odd thermal torkance $\beta_{xx}^{\text{odd}}$ are calculated for $T = 300$ K using Eq. (5), based respectively on $t_{yx}^{\text{even}}$ and $t_{xx}^{\text{odd}}$ from Fig. 3. The line of circles in the upper figure corresponds to the even thermal torkance $\beta_{yx}^{\text{SNE}}$ estimated from the spin Nernst conductivity of bulk fcc Pt, Eq. (9).

zeros of the thermal torkance correspond to the local extrema of the electrical torkance, while the maxima in the former correspond to the regions of largest slope of the latter. It is thus not surprising that the largest values of $\beta_{yx}^{\text{even}}$ of the order of tens of $\mu$eV $a_0$ K$^{-1}$ are achieved roughly 0.2 eV below the Fermi energy, while the magnitude of $\beta_{xx}^{\text{odd}}$ is maximal away from the Fermi energy, reaching as much as 100 $\mu$eV $a_0$ K$^{-1}$ there. Clearly visible in Fig. 5 is a much more pronounced dependence of the thermal torkances on the Pt thickness than in the case of the electrical torkances. The thermal torkances for six and 12/18 layers of the Pt substrate differ in sign over wide patches in energies around $-0.4$ eV and in the case of $\beta_{xx}^{\text{odd}}$ a larger difference between 12 and 18 Pt layers is observed when compared to $t_{xx}^{\text{odd}}$. At the true Fermi energy, $\beta_{xx}^{\text{odd}}$ exhibits a change of sign when changing the Pt thickness (see Table II).

It is known that in paramagnetic metals, in particular, Pt, an applied temperature gradient will result in a transverse spin current, analogous to the spin Hall current which is generated by an electric field. The respective phenomenon is called the spin Nernst effect (SNE) [28,29], and its magnitude is characterized by the spin Nerst conductivity (SNC) $\alpha$. Keeping in mind the geometry of our system, the relationship between a temperature gradient applied along the $x$ axis and the spin current density with spin polarization along the $y$ axis, which propagates along the $z$ axis, reads

$$j_z^y = -\alpha_{zx}^y \nabla T_x. \tag{8}$$

As in the previous section, we will compare the magnitude of the "pure" spin Nernst torkance $\beta_{yx}^{\text{SNE}}$ to the computed thermal torkance $\beta_{yx}^{\text{even}}$, assuming that the spin Nernst torkance arises from the full bulk spin Nernst current:

$$\beta_{yx}^{\text{SNE}} = S\alpha_{zx}^y. \tag{9}$$

To estimate the magnitude of the spin Nernst thermal torkance from *ab initio*, from the energy dependence of the SHC presented in Fig. 3, we evaluate the thermal intrinsic contribution to the SNC according to the Mott relation (at $T = 300$ K) [30,31]

$$\alpha_{zx}^y = -\frac{1}{e}\int d\mathcal{E}\frac{\partial f(\mathcal{E},\mu,T)}{\partial\mu}\sigma_{zx}^y(\mathcal{E})\frac{\mathcal{E}-\mu}{T}. \tag{10}$$

The spin Nernst thermal torkance $\beta_{yx}^{\text{SNE}}$ computed using Eqs. (9) and (10) is presented in Fig. 5 as a function of the position of the Fermi energy, together with $\beta_{yx}^{\text{even}}$. By comparing the two torkances we can conclude that, as in the case of the electrical torkances, the overall behavior of $\beta_{yx}^{\text{even}}$ with energy is in accordance with that of $\beta_{yx}^{\text{SNE}}$ in the window of energies between $-0.2$ and $+0.6$ eV. This hints at a clear correlation between the phenomenon of the TSOT and the SNE at these energies for our system. Owing to the essential energy dependence of the SHE-to-SOT efficiency $\xi$, the *SNE-to-TSOT efficiency* $\xi^T$, defined by relation $\beta_{yx}^{\text{even}} = \xi^T \beta_{yx}^{\text{SNE}}$, deviates quite significantly from $\xi$ and ranges approximately between 0.5 and 1.5 in the energy interval $[-0.2\text{ eV}, +0.6\text{ eV}]$, with the exception of energies where the torkances change sign (between 0.0 and 0.2 eV).

Since to the best of our knowledge the effect of TSOT has not been observed so far, it is important that we give an estimate of the TSOT that can be achieved experimentally in our films. We therefore compute the temperature gradient $|\nabla T|^0$ that is required to reproduce the total effective magnetic field obtained with the value of current density $j \sim 10^7$ A/cm$^2$, typical for experiments on such systems (Table II). The value of $|\nabla T|^0$ of the order of 2 K/nm which we obtain for our $L1_0$-FePt/Pt bilayers at their true Fermi energy turns out to be one order of magnitude larger than the one which can be achieved experimentally in this type of system [37]. This means that although the TSOT in the system that we study here most probably cannot be used to switch the magnetization, we conclude that the fingerprints of the effect can be observed.

We are, moreover, confident that at the current level of experimental techniques the TSOT can be made as large as the electrical SOT by proper electronic structure engineering, which can go along three different paths. (i) As apparent from Fig. 5, for FePt/Pt bilayers the thermal torkances can be order of magnitude larger if the Fermi energy is set to $\sim$0.6 eV above its true value—this corresponds roughly to using, e.g., $L1_0$-$(Fe_{1-x}Co_x)(Pt_{1-x}Au_x)$/$Pt_{1-x}Au_x$ instead of FePt/Pt, with $x \sim 0.6$ if we assume a constant density of states of $\sim$1 eV$^{-1}$ per atom for $Fe_{1-x}Co_xPt_{1-x}Au_x$ and $Pt_{1-x}Au_x$. (ii) Exploiting the close correlation between the TSOT and the SNE which we found, one could consider using fcc Ir, Pd, or Rh as substrates instead of fcc Pt, since the values of the intrinsic SNCs for these metals which we computed constitute $-8744$ (Ir), $+20\,804$ (Pd), and $-20\,779$ $(\hbar/e)\mu$A cm$^{-1}$ K$^{-1}$ (Rh), which is respectively $+1.04$, $-2.48$, and $+2.48$ times larger than the value of the SNC of fcc Pt of $-8383$ $(\hbar/e)\mu$A cm$^{-1}$ K$^{-1}$. (iii) Our calculations show that upon decreasing the disorder strength $\Gamma$, the energy dependence of the odd and, particularly, even torkances exhibits strong deviations from the smooth behavior shown above, acquiring sharp features and sign changes at the scale of tens of meVs. This effect is due to the fine features in the electronic structure of thin films, which get promoted as the band broadening is decreased. Correspondingly, upon reducing the degree of disorder in the system (e.g., by lowering of the temperature or concentration of impurities) the magnitude of the TSOT, qualitatively proportional to the degree of raggedness of the torkance as a function of energy, can be significantly enhanced, as confirmed by our calculations.

## V. CONCLUSIONS

Using expressions for the spin-orbit torkances derived from the Kubo linear response formalism, we compute from first principles the values of the even and odd torkances in a system consisting of two layers of ferromagnetic $L1_0$-FePt deposited on an fcc Pt(001) substrate of various thicknesses. We predict that the magnitude of the SOTs lies in the range of values measured experimentally and computed theoretically for Co/Pt bilayers. For both even and odd torques we find a pronounced energy and thickness dependence. By comparing the even SOT to that purely given by the spin Hall effect in the Pt substrate, we find that while around the Fermi energy the behavior of the two SOTs is very similar, they can differ in sign and order of magnitude for wide regions of energy. Moreover, using

the expressions that we derived recently for the thermal SOT, driven by the temperature gradient rather than the electric field, we compute the energy and thickness dependence of the thermal torkance in the system under consideration. We were also able to establish a close connection between the TSOT and the spin Nernst effect. We predict that thermal gradients of the order of 2 K/nm are necessary to exert the same torque on the magnetization as that arising from typical current densities in this kind of system, which assures us that the TSOT in FePt/Pt bilayers could be experimentally detected. We further speculate that much larger TSOTs can be achieved in other ferromagnetic transition-metal overlayers deposited on substrates which exhibit a larger spin Nernst effect than Pt.

## ACKNOWLEDGMENTS

We gratefully acknowledge computing time on the supercomputers JUQUEEN and JUROPA at Jülich Supercomputing Center as well as at the JARA-HPC cluster of RWTH Aachen, and funding under the HGF-YIG program VH-NG-513 and SPP 1538 of DFG.

[1] L. Berger, Phys. Rev. B **54**, 9353 (1996).
[2] J. Slonczewski, J. Magn. Magn. Mater. **159**, L1 (1996).
[3] J. Sun, J. Magn. Magn. Mater. **202**, 157 (1999).
[4] A. Chernyshov, M. Overby, X. Liu, J. K. Furdyna, Y. Lyanda-Geller, and L. P. Rokhinson, Nat. Phys. **5**, 656 (2009).
[5] I. M. Miron, T. Moore, H. Szambolics, L. D. Buda-Prejbeanu, S. Auffret, B. Rodmacq, S. Pizzini, J. Vogel, M. Bonfim, A. Schuhl *et al.*, Nat. Mater. **10**, 419 (2011).
[6] I. Mihai Miron, G. Gaudin, S. Auffret, B. Rodmacq, A. Schuhl, S. Pizzini, J. Vogel, and P. Gambardella, Nat. Mater. **9**, 230 (2010).
[7] A. Manchon and S. Zhang, Phys. Rev. B **79**, 094422 (2009).
[8] I. Garate and A. H. MacDonald, Phys. Rev. B **80**, 134403 (2009).
[9] I. M. Miron, K. Garello, G. Gaudin, P.-J. Zermatten, M. V. Costache, S. Auffret, S. Bandiera, B. Rodmacq, A. Schuhl, and P. Gambardella, Nature (London) **476**, 189 (2011).
[10] L. Liu, C.-F. Pai, Y. Li, H. W. Tseng, D. C. Ralph, and R. A. Buhrman, Science **336**, 555 (2012).
[11] L. Liu, O. J. Lee, T. J. Gudmundsen, D. C. Ralph, and R. A. Buhrman, Phys. Rev. Lett. **109**, 096602 (2012).
[12] S. Emori, U. Bauer, S.-M. Ahn, E. Martinez, and G. S. D. Beach, Nat. Mater. **12**, 611 (2013).
[13] K.-S. Ryu, L. Thomas, S.-H. Yang, and S. Parkin, Nat. Nanotechnol. **8**, 527 (2013).
[14] C. Hin Sim, J. Cheng Huang, M. Tran, and K. Eason, Appl. Phys. Lett. **104**, 012408 (2014).
[15] F. Freimuth, S. Blügel, and Y. Mokrousov, Phys. Rev. B **90**, 174423 (2014).
[16] F. Freimuth, S. Blügel, and Y. Mokrousov, J. Phys.: Condens. Matter **26**, 104202 (2014).
[17] E. S. Murdock, R. Simmons, and R. Davidson, IEEE Trans. Magn. **28**, 3078 (1992).
[18] P. Ravindran, A. Kjekshus, H. Fjellvåg, P. James, L. Nordström, B. Johansson, and O. Eriksson, Phys. Rev. B **63**, 144409 (2001).
[19] R. V. Chepulskii and W. H. Butler, Appl. Phys. Lett. **100**, 142405 (2012).
[20] M. M. Soares, H. C. N. Tolentino, M. De Santis, A. Y. Ramos, and J. C. Cezar, J. Appl. Phys. **109**, 07D725 (2011).
[21] S. Imada, A. Yamasaki, S. Suga, T. Shima, and K. Takanashi, Appl. Phys. Lett. **90**, 132507 (2007).
[22] T. Tanaka, H. Kontani, M. Naito, T. Naito, D. S. Hirashima, K. Yamada, and J. Inoue, Phys. Rev. B **77**, 165117 (2008).
[23] M. Onoda, G. Tatara, and N. Nagaosa, J. Phys. Soc. Jpn. **73**, 2624 (2004).
[24] P. M. Oppeneer, T. Maurer, J. Sticht, and J. Kübler, Phys. Rev. B **45**, 10924 (1992).
[25] L. D. Landau and E. M. Lifshitz, *Course of Theoretical Physics* (Pergamon, Oxford, UK, 1960), Vol. 8.
[26] D. Xiao, Y. Yao, Z. Fang, and Q. Niu, Phys. Rev. Lett. **97**, 026603 (2006).
[27] J. Weischenberg, F. Freimuth, S. Blügel, and Y. Mokrousov, Phys. Rev. B **87**, 060406 (2013).
[28] S.-g. Cheng, Y. Xing, Q.-f. Sun, and X. C. Xie, Phys. Rev. B **78**, 045302 (2008).
[29] X. Liu and X. Xie, Solid State Commun. **150**, 471 (2010).
[30] K. Tauber, M. Gradhand, D. V. Fedorov, and I. Mertig, Phys. Rev. Lett. **109**, 026601 (2012).
[31] S. Wimmer, D. Ködderitzsch, K. Chadova, and H. Ebert, Phys. Rev. B **88**, 201108(R) (2013).
[32] See http://www.flapw.de
[33] F. Freimuth, Y. Mokrousov, D. Wortmann, S. Heinze, and S. Blügel, Phys. Rev. B **78**, 035120 (2008).
[34] A. A. Mostofi, J. R. Yates, Y.-S. Lee, I. Souza, D. Vanderbilt, and N. Marzari, Comput. Phys. Commun. **178**, 685 (2008).
[35] K. Garello, I. M. Miron, C. O. Avci, F. Freimuth, Y. Mokrousov, S. Blügel, S. Auffret, O. Boulle, G. Gaudin, and P. Gambardella, Nat. Nanotechnol. **8**, 587 (2013).
[36] F. Freimuth, S. Blügel, and Y. Mokrousov, arXiv:1406.3866.
[37] A. Slachter, F. L. Bakker, J.-P. Adam, and B. Wees, Nat. Phys. **6**, 879 (2010).